Earth and Planetary Science Letters 389 (2014) 188–199

Contents lists available at ScienceDirect

Earth and Planetary Science Letters

www.elsevier.com/locate/epsl

Hafnium isotopic heterogeneity in zircons from granitic rocks: Geochemical evaluation and modeling of "zircon effect" in crustal anatexis

Ming Tang [a,b], Xiao-Lei Wang [a,c,*], Xu-Jie Shu [a], Di Wang [a], Tao Yang [a], Phillip Gopon [c]

[a] State Key Laboratory for Mineral Deposits Research, School of Earth Science and Engineering, Nanjing University, Nanjing 210093, China
[b] Department of Geology, University of Maryland, College Park, MD 20742, USA
[c] Department of Geoscience, University of Wisconsin, 1215 W. Dayton Street, Madison, WI 53706, USA

ARTICLE INFO

Article history:
Received 9 August 2013
Received in revised form 18 December 2013
Accepted 23 December 2013
Available online xxxx
Editor: T.M. Harrison

Keywords:
zircon effect
disequilibrium melting
modeling
Hf isotopes
zircon geochemistry
granitic rocks

ABSTRACT

We carried out a geochemical evaluation and modeled the mechanism responsible for varied Hf isotopic ratios in magmatic zircons of a single granitic rock specimen. Five representative granitic samples were selected from southern China based on preliminary Hf isotopic data. Our new dataset of zircon Hf isotopes confirmed significant Hf-isotope variations (5–9 epsilon units) for each sample, and these zircons show roughly positive Th/U versus T (crystallizing temperature) correlations, while the Lu/Hf variation is independent from T. In addition, some zircons show significantly higher Ti concentrations in the rims compared to the interiors, implying reverse thermal zonation based on the Ti-in-zircon thermometry. These geochemical features in zircons suggest open-system processes which may have resulted from frequent replenishment. We modeled zircon dissolution during crustal anatexis to reveal the Hf isotopic evolution in the extracted melts. The model suggests that the extracted melts may have extremely variable Hf isotope compositions (> 20 epsilon units) if the bulk Zr concentration in the source is initially above 100 ppm and the melting is rapid ($>10^{-4}$ yr^{-1}). The decoupled release of zircon Hf and non-zircon Hf from a single crust-derived magma source can lead to significant Hf-isotope variations in a solidified granitic body. This work provides an alternative explanation for the Hf isotopic heterogeneity in magmatic zircons of granitic rocks, which is in contrast to the common interpretation by mixing with mantle-derived magmas.

1. Introduction

The formation of continental crust is one of the main outcomes of planetary differentiation. The heterogeneity prevailing in the continental crust reflects the distinctive history of the entire crustal mass cycle—genesis, growth, evolution and reworking (Rudnick and Gao, 2003). Granitic batholiths and their erupted counterparts hold a significant portion of the continental landmass and harbor a record of the evolution of continental crust from birth to renewal. Understanding the formation and magmatic evolution of granitic rocks is the key to deciphering the processes involved in magmatic differentiation.

Radiogenic isotopes (e.g., Sr, Nd, Pb, and Hf isotope systematics) have been demonstrated to be powerful tools in tracing magmatic differentiation as they provide reliable indexes of mass transfer between isotopically distinct sources. In particular, the application of the Hf isotope system by Multi-collector Inductively Coupled Mass Spectrometry (MC-ICP-MS) has expanded greatly in recent years with the advent of effective Laser Ablation ICP-MS (LA-ICPMS) analysis of zircon, and has significantly furthered our insights into granitic magmatism with finer spatio-temporal resolution (e.g., Kinny and Mass, 2003; Flowerdew et al., 2006; Kemp et al., 2007; Wang et al., 2013).

Zircon grows by adding zones to its periphery, and these zones record the compositions of the melt as a function of time. An interesting and commonly observed phenomenon is that zircon Hf-isotope compositions can be highly heterogeneous even within a single specimen. Many scholars interpreted it as evidence of mixing of magmas from different sources, especially the incorporation of mantle-derived magmas into granitic magmas (e.g., Griffin et al., 2002; Belousova et al., 2006; Kemp et al., 2007; Nebel et al., 2007; Chen et al., 2008; Shaw and Flood, 2009; Sun et al., 2010). However, many of these interpretations assume equilibrium melting, which is seldom seen.

Zircon is a ubiquitous, Hf-enriched mineral in the continental crust. Its high stability and extremely low Lu/Hf ratio may result in preferential retention of Hf relative to Lu during chemical

* Corresponding author at: State Key Laboratory for Mineral Deposits Research, School of Earth Science and Engineering, Nanjing University, Nanjing 210093, China. Tel.: +86 2589680896; fax: +86 2583686016.
E-mail address: wxl@nju.edu.cn (X.-L. Wang).

0012-821X/$ – see front matter
http://dx.doi.org/10.1016/j.epsl.2013.12.036

weathering of continental crust. This may give rise to the decoupling of the Hf isotope system from other radiogenic isotope systems. The term "zircon effect" was first introduced by Patchett et al. (1984) to explain the Hf–Nd isotopic decoupling during chemical weathering, and has significant implications for discussing crustal recycling (Patchett et al., 1984). It has been observed in granitoids (Wu et al., 2006; Zheng et al., 2008), subduction zone magmas (Hanyu et al., 2006; Carpentier et al., 2009; Hoffmann et al., 2011), and mantle metasomatism (Roux et al., 2009; Yu et al., 2009; Tappe et al., 2011; Choi and Mukasa, 2012). However, less attention has been paid to the zircon effect on Hf systematics in crustal melting. In this work we extend the idea of "zircon effect" to crustal anatexis. We suggest that zircon dissolution is a complete disequilibrium process in terms of Hf. We also modeled the impact of the zircon effect on Hf isotopic systematics in single-sourced granitic magmatism. We propose that the decoupled release of zircon Hf and non-zircon Hf at the source may lead to highly variable Hf isotopic composition in the extracted melts.

2. Sample description

Southern China is one of the largest granite terranes in the world, with a total outcrop area of granitic rocks of ~160,000 km^2 (Zhou et al., 2006) and ages ranging mainly from ca. 910 Ma to ca. 90 Ma (Ye et al., 2007; Wang et al., 2006; Zhou et al., 2006). Abundant U–Pb and Hf isotope analyses have been carried out on zircons from these granitic rocks over the past five years (e.g., Qi et al., 2007; Zhao et al., 2010; Qiu et al., 2012; Chen et al., 2013; Shu et al., 2013; Zhu et al., 2013). Based on a compilation of published data and our Hf isotope data, five representative samples from four granitic plutons were selected for the geochemical evaluation of this study. These samples were selected based on their significant Hf isotopic heterogeneity (>5 epsilon units).

Samples 09JL-6-1 (28°46′17.3″N, 114°57′41.9″E) and 09JL-11-1 (28°33′23.8″N, 114°51′36.3″E) are strongly peraluminous (aluminum saturation index higher than 1.1) quartz diorite and biotite granite, respectively, collected from the same Neoproterozoic (ca. 820 Ma; Li et al., 2003; Wang et al., 2013) Jiuling Pluton (south-central China). Some cordierites were found in sample 09JL-6-1. A few biotite-enriched enclaves and dark granular diorite enclaves have been described in the southern part of Jiuling Pluton (Yu et al., 2006) but no enclaves were found near our sampling locations. Sample JS-8 (24°41′47.4″N, 117°17′50.6″E) is a biotite monzogranite collected from the Longshan Pluton (ca. 105 Ma; Li et al., 2009) of the Jinshan granite suite. Sample 07BLS-3 (25°28′41.9″N, 112°49′43.0″E) is a fine-grained biotite granite from the Qitianling Pluton (ca. 150 Ma; Shu et al., 2011) of the Mesozoic low Nd model age granite belt, with $\varepsilon_{Hf}(t)$ (see Supplementary file 1 for calculation method) variation in zircons spreading up to 8 epsilon units (Shu et al., 2011). Sample 08HF-6 (26°20′04.6″N, 117°27′25.1″E) is a medium- to coarse-grained biotite granite collected from the Shaxi intrusion of the Hufang composite granitic pluton (ca. 410 Ma; Li et al., 2010), which is exposed in the Qiuliu–Mingxi area of western Fujian Province, China. A few microgranular enclaves were observed in the Shaxi intrusion but the enclaves were absent at the sampling location (Li et al., 2010).

3. Analytical techniques

Zircon grains were separated from the five samples for *in situ* analyses. Cathodoluminescence (CL) or back-scattered electron (BSE) images were taken for each zircon grain. Most zircon grains were measured in both the core and rim domains for comparisons of Th, U, Ti concentrations, calculated Ti-in-zircon temperatures, and Hf isotopes between the core and rim.

3.1. Zircon U–Th–Pb isotopes and [Ti]

Zircon U–Th–Pb isotopes and [Ti] (Ti concentrations) were analyzed simultaneously using an Agilent 7500a Q-ICP-MS coupled with a New Wave UP213 laser ablation system at the State Key Laboratory for Mineral Deposits Research (MiDeR), Nanjing University (NJU). Nine isotopes including ^{238}U, ^{232}Th, ^{208}Pb, ^{207}Pb, ^{206}Pb, ^{139}La, ^{172}Yb, ^{29}Si and ^{49}Ti were measured. Dwell time for each isotope was: 10 ms for ^{232}Th, ^{208}Pb, ^{139}La, ^{172}Yb and ^{29}Si; 15 ms for ^{206}Pb and ^{238}U; 30 ms for ^{207}Pb; 50 ms for ^{49}Ti. Dating results are reported in 1σ.

The National Institute of Standards and Technology (NIST) SRM-612 glass was chosen as the standard reference material for trace element concentrations, since its relatively low [Ti] of 44 ppm (Jochum et al., 2011) roughly matches the [Ti] in most zircons, and it could provide enough signal intensity to allow precise calibration. The low abundance isotope ^{49}Ti was measured to eliminate isobaric interferences. ^{29}Si was assigned as the internal standard. Discussion of analytical challenges of *in situ* zircon [Ti] measurement and detailed description of our analytical techniques are available in Supplementary file 1.

3.2. Zircon Ti thermometry

Zircon Ti temperatures were calculated according the equation proposed by Watson and Harrison (2005). Because the geological meaning of these calculated temperatures is debated (e.g., Nutman, 2006; Fu et al., 2008; Harrison et al., 2007), we use them simply to compare the crystallization temperatures of our samples. Estimations of Si and Ti activities are required before applying the Ti-in-zircon thermometry of Watson and Harrison (2005). All of the studied samples are relatively SiO_2-rich ($SiO_2 \geqslant 63$ wt.%) and quartz-bearing, suggesting that a_{SiO_2} was high during crystallization. For simplicity, we assumed the activity of SiO_2 (a_{SiO_2}) to be 1 during zircon growth. An overestimate of a_{SiO_2} by 0.15 results in an overestimate of temperature by less than 20 °C. a_{TiO_2} is difficult to assess accurately. However, a_{TiO_2} of most silicate igneous rocks varies between 0.6 and 0.9 (Hayden and Watson, 2007), and no rutile was found in our samples, which indicates Ti undersaturation in the magmas. Therefore, we chose the mid-point value (0.75) as the a_{TiO_2} for the calculations. 0.15 units of a_{TiO_2} at 10 ppm Ti leads to either an under- or over-estimate of temperature by ca. 20 °C (Ickert et al., 2010). It should be pointed out that our emphasis is placed on the temperature variations across individual zircons within each magmatic system, whose a_{TiO_2} should broadly remain constant during zircon crystallization. Comparisons of zircon Ti temperature between different plutons are not intended here. Thus, a loosely constrained a_{TiO_2} would not hamper our discussion.

3.3. Zircon Hf isotopes

Zircon Hf isotopes were analyzed using a Neptune (Plus) MC-ICP-MS attached to a New Wave ArF 193 nm laser ablation system at MiDeR-NJU. He and Ar were used as the carrier gases to transport the ablated materials to the ICP torch. Spot analyses were conducted using a 35 μm beam at 8 Hz or a 50 μm beam at 5 Hz repetition rate. A new TIMS (thermal ionization mass spectrometer)-determined value of 0.5887 for ^{176}Yb/^{172}Yb was applied for a correction of mass bias (Vervoort et al., 2004). Each analyzing cycle included a 5-second background measurement followed by 25-second sample ablation. For each spot 200 analyses can be obtained, and the mean ^{176}Lu/^{177}Hf, ^{176}Yb/^{177}Yb and ^{176}Hf/^{177}Hf ratios are calculated. Reference zircon Mud Tank (MT) (^{176}Hf/^{177}Hf = 0.282507 ± 6; Woodhead and Hergt, 2005) was analyzed after 3 to 5 unknowns to monitor instrument stability.

Table 1
Summary of the variations of Th and U concentrations, Th/U ratios, $\varepsilon_{Hf}(t)$ and Ti-in-zircon temperatures for the five representative samples of this study.

	Th (ppm)	U (ppm)	Th/U	$\varepsilon_{Hf}(t)$	Temperature (°C)
09JL-11-1	25–643	131–885	0.09–1.09	(−0.8)–(+8.2)	671–825
09JL-6-1	31–259	85–371	0.10–1.05	(+1.3)–(+6.5)	689–822
JS-8	93–4676	124–5988	0.44–1.60	(−2.8)–(+3.5)	657–818
07BLS-3	75–705	114–2907	0.11–0.74	(−11.1)–(−3.9)	708–870
08HF-6	49–986	92–1448	0.09–1.82	(−11.0)–(−2.6)	607–883

A total of 111 analyses of MT zircon in this study yielded a mean $^{176}Hf/^{177}Hf$ ratio of 0.282508 ± 4 (95% conf.). The decay constant for ^{176}Lu of 1.865×10^{-11} yr^{-1} proposed by Scherer et al. (2001) was adopted in this work. ε_{Hf} values were calculated according to the chondritic values of Blichert-Toft and Albarede (1997). The equation to calculate $\varepsilon_{Hf}(t)$ is available in Supplementary file 4.

4. Results

4.1. Geochronology

U–Pb dating was carried out to ensure that the zircons used for Hf isotopic analysis are of the same ages within each rock sample. Discordant results (discordance % > 5%) were excluded in age calculations. Only the analyses that clustered in a group are calculated for the weighted average ages (Table 1), and only the analyses within the age groups were taken for comparisons in [Ti] and Hf isotopes. 96 analyses of sample 09JL-6-1 yielded a mean $^{206}Pb/^{238}U$ age of 813.5 ± 2.5 Ma (95% conf., MSWD = 0.82). 54 analyses of sample 09JL-11-1 yielded a mean $^{206}Pb/^{238}U$ age of 818.6 ± 3.7 Ma (95% conf., MSWD = 1.4). The two ages are consistent with the previously published U–Pb ages for the Jiuling Pluton (ca. 820 Ma; Li et al., 2003; Wang et al., 2013) within uncertainty. 92 analyses were obtained for sample JS-8 and yielded a mean $^{206}Pb/^{238}U$ age of 105.8 ± 0.4 Ma (95% conf., MSWD = 1.4). 78 analyses were obtained for sample 07BLS-3 and yielded a mean $^{206}Pb/^{238}U$ age of 148.5 ± 0.7 Ma (95% conf., MSWD = 1.6). 48 analyses of sample 08HF-6 yielded a mean $^{206}Pb/^{238}U$ age of 412.7 ± 1.9 Ma (95% conf., MSWD = 1.3). Zircon U–Pb isotopes and concordia diagrams are available in Supplementary files 1 and 2.

4.2. Zircon geochemistry and Ti-in-zircon thermometry

The Th/U ratios, calculated $\varepsilon_{Hf}(t)$, and Ti-in-zircon temperatures all show large variations for individual samples. A brief summary of the results is provided in Table 1. Zircon Ti thermometry results indicate that most zircons from these granitic rocks crystallized between 650 °C and 850 °C. Unlike zircon saturation thermometry which may provide an estimate of melting temperature (minimum or maximum depending on the presence of inherited zircon) at the source for granitic rocks (e.g., Miller et al., 2003; Harrison et al., 2007), the results of Ti-in-zircon thermometry only record the thermal information when the zircon is crystallizing, and should not be used to infer the initial melting temperature (Nutman, 2006). Generally, granitic magma reaches late-stage evolution when temperature approaches 650 °C, close to the solidus of wet granite (Tuttle and Bowen, 1958). Interestingly, each of the five samples has some analyses with Ti-in-zircon temperatures as low as 650 °C. Such a wide temperature spectrum (from over 800 °C to 650 °C) implies zircon growth spans much of the crystallization interval of felsic magmas (Harrison et al., 2007). Only the zircons with concordant ages (discordance % < 5%) were analyzed for Hf isotopes. Our data show that all of the five samples have heterogeneous zircon Hf isotopic compositions (> 5 epsilon units). Zircon trace elements and Lu–Hf isotope data are provided in Supplementary files 3 and 4, respectively.

5. Discussion and modeling

5.1. Open system recorded by reverse thermal zonation

Hoskin and Schaltegger (2003) proposed Th/U ratio as a tool to distinguish between magmatic and metamorphic zircon, and concluded that typical magmatic zircons have Th/U ratios greater than 0.5 and metamorphic zircons commonly lower than 0.1. In this work, relatively low Th/U ratios (0.1–0.5) were usually obtained on the zircon rims. However, it would be difficult to attribute these low Th/U domains to metamorphic recrystallization since there is no evidence of metamorphism in the studied granitic bodies, and the U–Pb ages are concordant and consistent with high Th/U interior domains. Furthermore, the zircons show parallel zonation, and there are no signs suggesting secondary growth or recrystallization (Fig. S1 in Supplementary file 1).

Theoretically, magma temperature decreases with increasing magmatic differentiation. But open-system processes may interrupt the monotonic cooling as the magma chamber may be recharged (Claiborne et al., 2006, 2010a, 2010b; Ickert et al., 2010). In this case, the interiors and rims of zircons may record the temperatures and compositions of magmas from different recharge events, which may result in reverse temperature zonation across individual zircon grains. This reverse zonation exists in all of the studied samples but is least common in sample 09JL-6-1.

5.2. Zircon Th/U– and Lu/Hf–T: temperature effect, crystallization and replenishment?

Trace element ratios (e.g., Th/U and Lu/Hf) in zircons are controlled by elemental partitioning thermodynamics and the ratios in the melt. The correlation between zircon Th/U ratio and *T* (temperature) (Fig. 1a2, b2, c2, d2 and e2) has been recognized by previous studies (e.g., Harrison et al., 2007; Claiborne et al., 2010a, 2010b). Harrison et al. (2007) interpreted the low Th/U in zircons formed at low temperatures as a result of co-crystallization of monazite. However, temperature has been shown to be an important factor controlling the trace element partitioning into zircons (Rubatto and Hermann, 2007; Zhang et al., 2010), and thus trace element ratios in zircon. In Supplementary file 1, we used the equation proposed by Blundy and Wood (1994) to show that U becomes increasingly more compatible than Th in the zircon lattice with decreasing temperature. The positive correlation between zircon Th/U and *T* likely reflects the combined effect of temperature and co-crystallization of monazite. The various degrees of scatter may result from magma replenishment, which can cause significant heterogeneity. This may be further linked to accessory phase dissolution at the source, which controlled the release of trace elements into the melts. The lack of correlation between Lu/Hf ratio and *T* (Fig. 1a3, b3, c3, d3 and e3) may indicate even stronger heterogeneity of Lu/Hf in the melt and especially the variable behavior of Lu because Hf has been shown to have a good negative correlation with Ti (or Ti-in-zircon temperature) in zircon (Claiborne et al., 2010a, 2010b). It also needs to be pointed out that Hf partitioning behavior may significantly deviate from a Henry's Law type due to its high concentration in zircon (Claiborne et al., 2006),

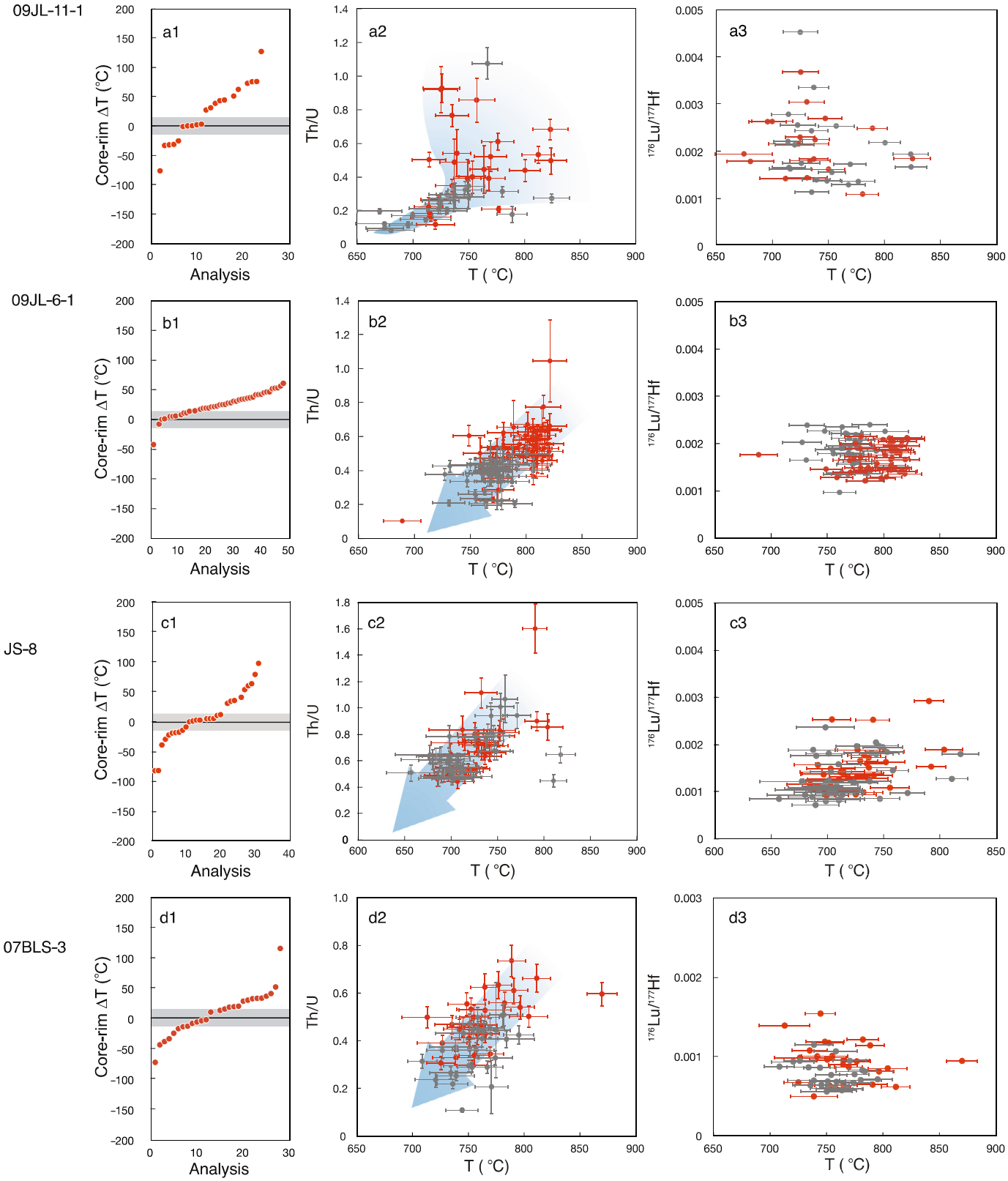

Fig. 1. a1, b1, c1, d1 and e1: Core-rim temperature differences (core-rim $\Delta T = T_{core} - T_{rim}$) for individual zircon grains. The grey belt indicates typical analytically indistinguishable areas. Zircons that fall below the grey belt have reverse thermal zonation; a2, b2, c2, d2 and e2: Correlation between zircon Th/U and temperature; a3, b3, c3, d3 and e3: Plots of $^{176}Lu/^{177}Hf$ vs. temperature. Red dots denote the core analyses and grey dots denote the rim. Error bars are $2\sigma_m$, and the error bars of $^{176}Lu/^{177}Hf$ are within the dots. (For interpretation of the references to color in this figure legend, the reader is referred to the web version of this article.)

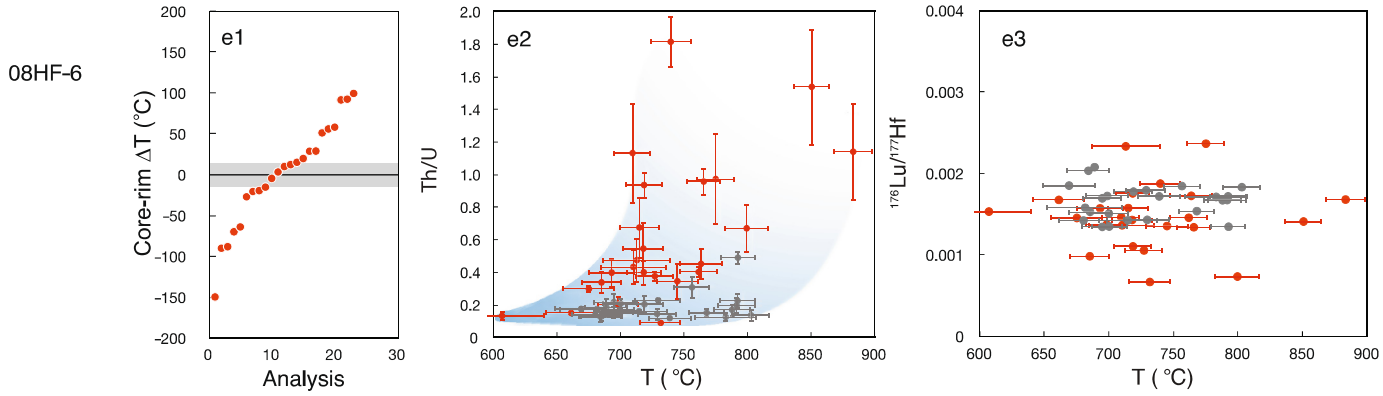

Fig. 1. (*continued*)

which further complicates the situation beyond the melt composition and temperature effects.

For the samples considered here, there is currently no clear field evidence (e.g., mafic microgranular enclaves, disequilibrium mineral pairs, and accompanying mafic intrusions) indicating mantle input. Moreover, zircon $\varepsilon_{Hf}(t)$ variation, which is independent from zircon Th/U ratio, fails to resolve any mixing of mantle-derived magmas (Fig. 2). We compared the $\Delta\varepsilon_{Hf}(t)_{core\text{-}rim}$ of each zircon that has reverse thermal zonation (Fig. 3), and found that the high-temperature rims are not more radiogenic (depleted mantle like) than the low-temperature cores. Furthermore, the *in situ* oxygen isotope results indicated small variations of zircon $\delta^{18}O$ (6.5–8.0‰; Wang et al., 2013) in 09JL-11-1, which is decoupled from the variation of zircon $\varepsilon_{Hf}(t)$ (see Fig. S3 in Supplementary file 1). Although sample 09JL-11-1 and sample 09JL-6-1 were collected from the same pluton, their different geochemical characteristics in zircons may reflect distinct magma chamber processes. Compared with sample 09JL-6-1, sample 09JL-11-1 is characterized by more scatter in the Th/U–T plot (Fig. 1), greater variation in $\varepsilon_{Hf}(t)$ and Lu/Hf ratios, and more grains with reverse thermal zonation. These observations point to a more active magma chamber with frequent replenishment for sample 09JL-11-1.

5.3. Isotopic disequilibrium during crustal anatexis

One of the fundamental assumptions that enable the utility of isotopic tracers to infer source composition is that melt reaches isotopic equilibrium with protoliths during partial melting. This could be accomplished in two ways: 1) All phases in the source break down simultaneously and are melted proportionally; and 2) The closure temperature is reached for all phases and isotopic exchange between the melt and residue is rapid and sufficient.

The first situation is unlikely to happen since mineral dissolution/growth is dictated by melt composition, temperature, pressure, etc. The second situation depends on the diffusivity of the isotopes in various phases and the timescale of melt-residue interaction before extraction. Indeed, progressively more studies have reported significant Sr, Nd, and Pb isotopic disequilibrium during crustal anatexis (e.g., Hogan and Sinha, 1991; Hammouda et al., 1994; Knesel and Davidson, 1996; Ayres and Harris, 1997; Tommasini and Davies, 1997; Davies and Tommasini, 2000; Zeng et al., 2005a, 2005b; Farina and Stevens, 2011). Lutetium and Hf may reside primarily in garnet and zircon, respectively. Dissolution of these minerals at the source may control the release of radiogenic ^{176}Hf and unradiogenic ^{177}Hf to the melt. If Hf diffusivity in zircon is not rapid enough to reach equilibrium, the Hf isotope composition of the melt will be highly sensitive to the zircon dissolution rate during crustal anatexis (Flowerdew et al., 2006). The zircon dissolution rate is controlled by several factors such as zircon solubility, temperature, zircon crystal size, and the melt and solid phase composition. The varying zircon dissolution rate at a single magma source may result in varying Hf isotope compositions between different batches of melts.

5.4. Inter-mineral Hf isotopic variation and Hf diffusivity in zircon

We calculated the inter-mineral isotopic difference relative to zircon (termed as $\Delta\varepsilon Hf_{X\text{-}zircon}$) as a function of crustal residence time (Fig. 4). Assuming Lu–Hf isotope systematics in these minerals remain closed prior to melting, the isotope difference between garnet and zircon may grow in excess of 200 epsilon units after 500 Ma. As long as slow diffusion rates fail to homogenize the isotope composition between the melt and each phase, disequilibrium melting would occur. Using the Hf diffusion coefficient in zircon provided by Cherniak et al. (1997), we calculated the zircon Hf diffusion length as:

$$l_d = \sqrt{Dt} \tag{1}$$

where l_d is the zircon Hf diffusion length in meter, D (in m^2/s) is the Hf diffusion coefficient in zircon and t is the timescale of a crustal melting event in seconds. The timescale of crustal partial melting generally ranges from 1 Ma to 100 years (Petford et al., 2000 and the references therein). Fig. 5 plots the diffusion length (in μm) of Hf in zircon as a function of timescale and crustal melting temperature. Hafnium diffuses only 1 nm over 1 Ma even when the temperature is maintained as high as 950 °C. We thus conclude that the diffusive exchange of Hf between melt and zircon is negligible, and the release of zircon Hf is solely controlled by zircon dissolution during partial melting.

5.5. Zircon dissolution during crustal anatexis: modeling

Since Hf diffusion coefficients are currently unknown for phases other than zircon during crustal melting, we applied a dynamic crustal melting model and considered two extreme scenarios: 1) complete disequilibrium melting (negligible diffusive exchange of Hf and Zr between the melt and residual phases) for all phases; and 2) complete equilibrium melting for all phases except zircon.

For the modeling, we assume that:

1) Steady melting occurs when temperature continuously increases from 750 °C to 950 °C with a maximum melting degree of 40% reached at the peak temperature;
2) Once the melt fraction reaches the critical porosity (φ) (10% in our case) in the source region, the melt is continuously extracted from the source by deformation-assisted segregation so as to maintain a constant porosity (e.g., Sawyer, 1994). The extracted melt is chemically isolated from the source.

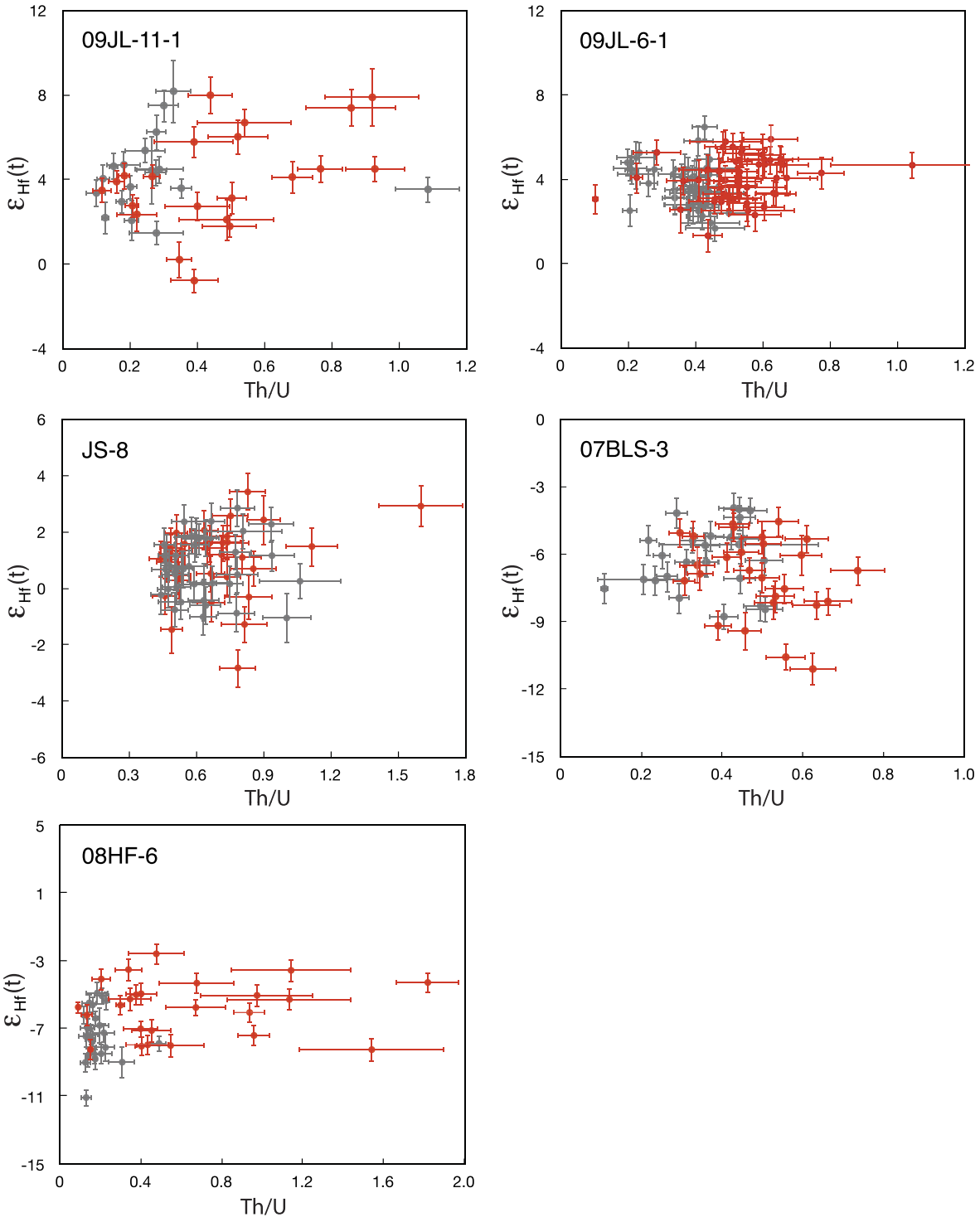

Fig. 2. Plots of zircon $\varepsilon_{Hf}(t)$ vs. Th/U. Error bars are $2\sigma_m$.

3) Whole-rock Zr concentration ranges from 50 to 200 ppm. The source matrix is initially in equilibrium with zircon at 650 °C;
4) A melt cation ratio $M = 1.3$ (Watson and Harrison, 1983) was used in the calculation. The density difference between the melt and the solid was ignored. The bulk Zr and Hf partition coefficients are 0.3;
5) During complete equilibrium melting, all phases (except zircon) are in equilibrium with the residual melt at all times;
6) All zircons are spherical and are in contact with the melt at all times.

The melt in the source matrix can start to move once there is 10% to 20% melt (Sawyer, 1994). Although the porosity used in our calculation is 10%, the model presented here is fairly insensitive to this parameter (<10% variation by changing porosity from 10% to 20%). The third assumption provides a rough estimate of Zr distribution between zircon and the matrix. Generally, most Zr resides in zircon (Miller et al., 2003). The assumption for modal melting significantly simplifies the situation. However, a more accurate description of disequilibrium melting requires knowledge of the melting reactions that consider both major and accessory

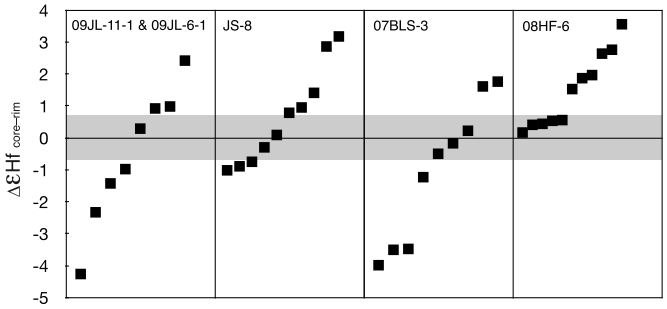

Fig. 3. Core-rim $\varepsilon_{Hf}(t)$ difference for zircon grains with reverse thermal zonation. The gray shaded band indicates typical analytical uncertainty at $2\sigma_m$ level.

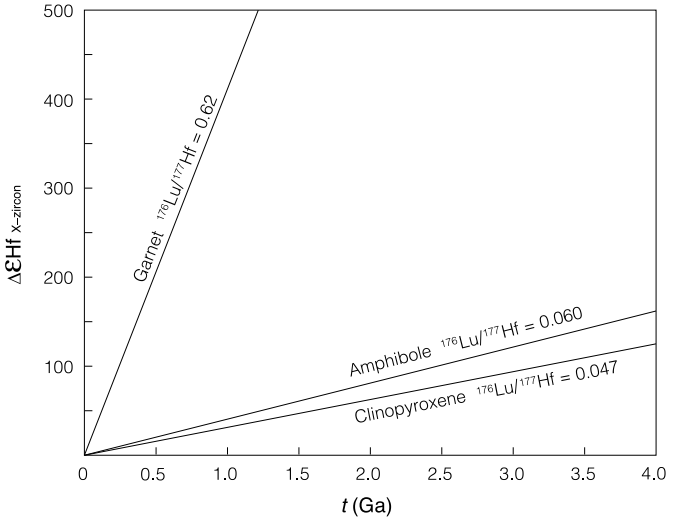

Fig. 4. Inter-phase ε_{Hf} differences relative to zircon due to decoupled ingrowth of radiogenic ^{176}Hf. It is assumed that the initial Hf isotope composition is homogeneous and that the Lu–Hf isotope systems remained closed during crustal residence. Note that such inter-phase Hf isotope differences grow rapidly between garnet and zircon, of which, garnet controls Lu and thus ^{176}Hf in the bulk system while zircon holds the budget of the total Hf. Accessory minerals such as apatite and monazite, which are REE enriched and have high $^{176}Lu/^{177}Hf$ ratios (Kinny and Mass, 2003), are not plotted here. $^{176}Lu/^{177}Hf$ ratio in garnet from Anczkiewicz et al. (2007); $^{176}Lu/^{177}Hf$ ratio in amphibole from Wang et al. (2012); $^{176}Lu/^{177}Hf$ ratio in clinopyroxene from Jagoutz et al. (2007). The $^{176}Lu/^{177}Hf$ ratio in zircon is assumed to be 0.001.

phases, which is yet to be obtained. The cation ratio (M) of 1.3 suggested by Watson and Harrison (1983) is a typical value for peraluminous granite. The model presented below is robust to the variation of M within a geologically reasonable range. Assumption (6) may not be true during the early stage of melting because zircon may be hosted in other phases such as biotite at that time (Bea, 1996). Dissolution will not begin until zircon physically contacts the melt. Therefore, this assumption may overestimate the effective dissolution rate of zircon. The notation used in the model are detailed in Table 2.

The instant dissolution rate of spherical zircon crystals is given by Watson's equation (Watson, 1996):

$$\frac{dr}{dt} = U \cdot \left[\left(\frac{1.25 \cdot 10^{10}}{r} \right) e^{\frac{-28380}{T}} + 7.24 \cdot 10^{8} e^{\frac{-23280}{T}} \right] \cdot 10^{-17} \quad (2)$$

where

$$U = C_{sat} - C_l, \quad (3)$$

$$C_{sat} = D_{Zr}^{zircon/melt} C_{Zr}^{zircon}, \quad (4)$$

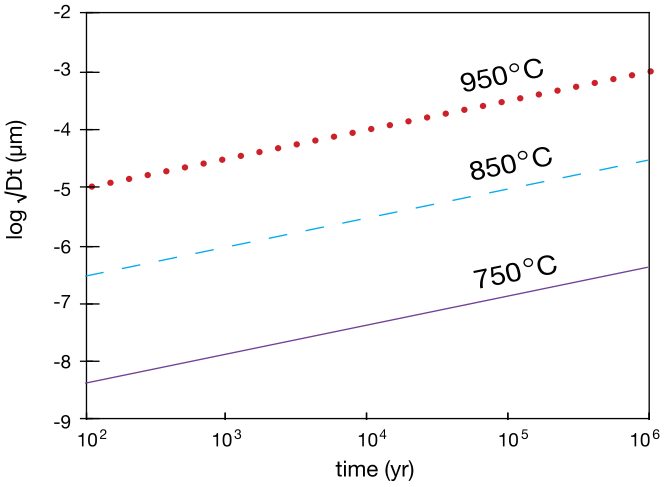

Fig. 5. Hafnium diffusion length in zircon as a function of timescale of anatexis under crustal melting temperatures. Under crustal melting temperatures, Hf essentially doesn't diffuse in zircon.

Table 2
Notation used in modelling.

Variable	Description	Dimension
T	temperature	K
T_0	temperature at the onset of melting	K
T_p	temperature at the thermal peak	K
τ	timescale of partial melting	yr
t	time	s
F	maximum melting degree	none
f	melt fraction	none
r_0	initial zircon radius	μm
r	zircon radius	μm
C_l	Zr concentration in the residual melt	ppm
$C_{s,0}$	initial Zr concentration in the solid without zircon	ppm
C_s	Zr concentration in the solid without zircon	ppm
C_w	initial whole-rock Zr concentration	ppm
C_{sat}	Zr concentration in the melt saturated in zircon	ppm
V_l	normalized residual melt volume	none
V_s	normalized solid volume	none
D_{Zr}	bulk Zr partition coefficient	none
v_m	normalized melting rate	yr^{-1}
v_e	normalized melt extraction rate	yr^{-1}
φ	porosity	none
M	melt cation ratio	none

$$\ln D_{Zr}^{zircon/melt} = -3.8 - \left[0.85(M-1)\right] + \frac{12900}{T} \quad (5)$$

(Watson and Harrison, 1983).

Zirconium concentration in the residual melt is given by:

$$\frac{d(C_l V_l)}{dt} = \frac{4}{3}\pi \frac{d(r/r_0)^3}{dt}(C_w - C_s) + \frac{d(C_s V_s)}{dt} - C_l v_e. \quad (6)$$

For equilibrium melting:

$$\frac{C_s}{C_l} = D_{Zr}. \quad (7)$$

For complete disequilibrium melting:

$$C_s = C_{s,0}. \quad (8)$$

Based on the first and second assumptions, we have

$$\frac{dT}{dt} = \frac{T_p - T_0}{\tau} \quad (9)$$

and

$$\frac{dV_l}{dt} = v_m - v_e. \quad (10)$$

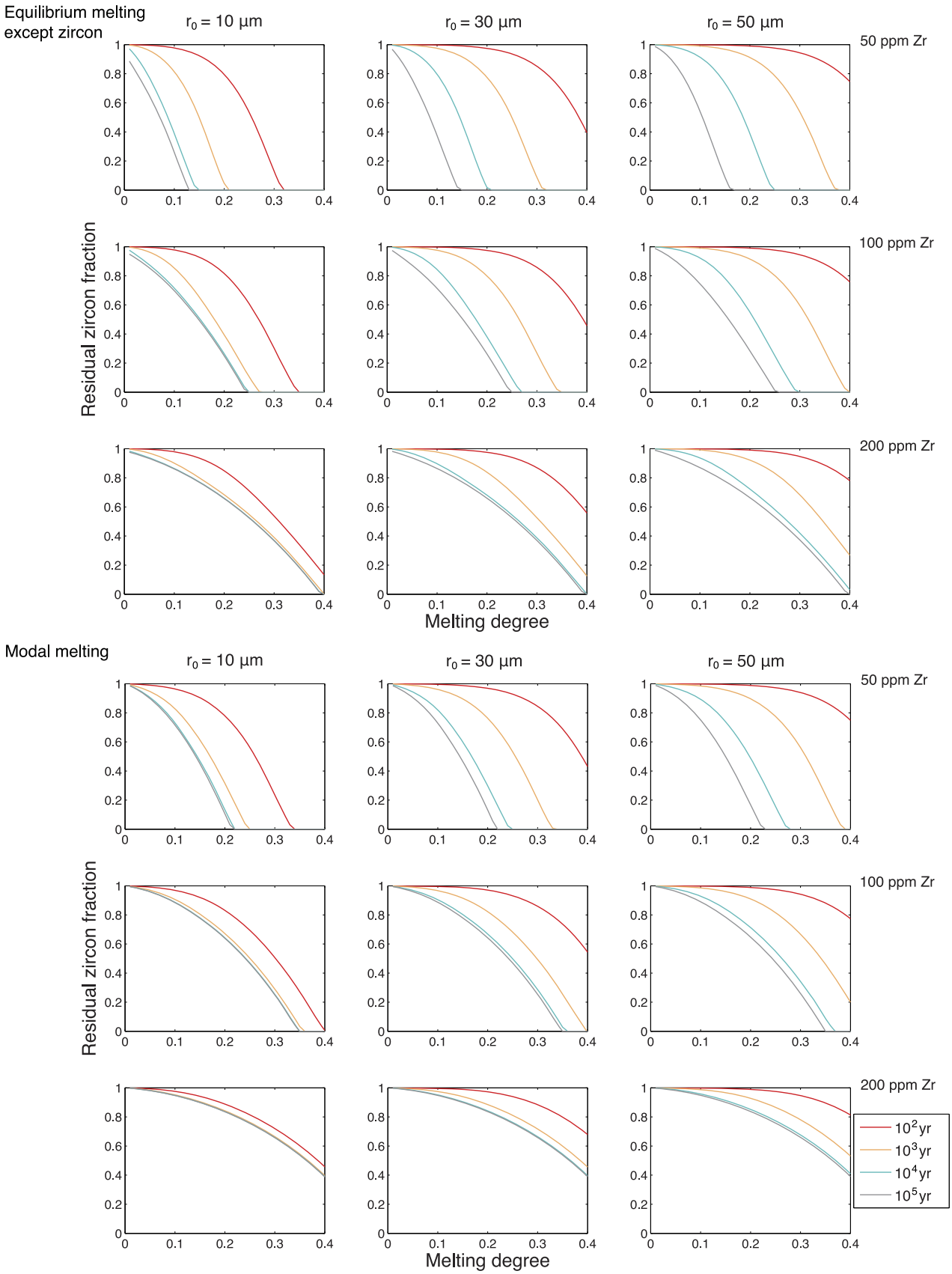

Fig. 6. Residual zircon fraction at various degrees of melting. Timescales of partial melting are indicated by the colors of the curves. The results become less sensitive to the melting rate when the initial Zr content is high. We calculated the curves for even longer melting timescales, but didn't plot them here because they mostly overlap with the 10^5 yr curve. Generally, zircon dissolves slower in the modal melting model. This is because the assumed zero diffusive exchange between the solid and melt translates into a bulk distribution coefficient of 0 for the Zr from dissolved zircon. The net result is more enriched Zr in the residual melt. (For interpretation of the references to color in this figure legend, the reader is referred to the web version of this article.)

The melting degree f is related to normalized melting rate v_m by:

$$f = v_m t. \tag{11}$$

When $f \leqslant \varphi$,

$$\frac{v_e}{v_m} = 0. \tag{12a}$$

When $f > \varphi$,

$$\frac{v_e}{v_m} = \frac{1}{1-\varphi}. \tag{12b}$$

Boehnke et al. (2013) updated Eq. (5) but the difference is trivial at 750–950 °C. Eq. (6) states the mass conservation: the change in the amount of Zr in the residual melt is determined by zircon dissolution, mass exchange between the melt and the solid matrix, and melt extraction. Eqs. (2)–(12) were solved numerically.

Fig. 6 shows the evolution paths of residual zircon fractions for zircons of three initial radii (10, 30 and 50 μm) and three initial whole-rock Zr concentrations (50, 100 and 200 ppm). Three main conclusions may be drawn from this figure. First, large zircon grains dissolve slower than small ones. Such a "size effect" becomes more important when the melting at the source is fast. Second, zircon dissolution is significantly affected by initial whole-rock Zr contentrations. This is because high Zr concentrations at the source can easily saturate the melt with zircon and zircon dissolution will stop until more melt is generated to dilute the remaining Zr at the source. Third, the melting rate at the source, as indicated by the timescale of melting, becomes less important with increasing initial whole-rock Zr concentration. Notice that, under any of the circumstance considered here, zircons cannot be completely dissolved at 10% melting when melt extraction occurs. If the initial Zr concentration of the source is above 200 ppm, even the smallest zircon can survive the 40% melting of the source.

As the major carrier of Hf, zircon (if present) will control the Hf budget at the source, and its dissolution may dictate Hf isotopic evolution in the melt. Undissolved zircon may retain a significant amount of ^{177}Hf at the source. We now link the relationship between the Hf isotope composition in the extracted melt and zircon dissolution by assuming that (1) the source rock has a crustal residence age of 1 Ga and (2) the bulk ε_{Hf} is −5 at the beginning of melting. Fig. 7 shows the evolution of ε_{Hf} in the extracted melt that continuously feeds the magma chamber. These evolution paths delineate the maximum ε_{Hf} variation that may be captured by the zircons crystallizing in the magma chamber. In both cases (i.e., complete disequilibrium and equilibrium matrix melting) ε_{Hf} variation increases with increasing initial whole-rock Zr concentrations. When the initial Zr concentration at the source is sufficiently high (e.g., >100 ppm), the inter-batch Hf varies from low-concentration and highly radiogenic to high-concentration and less radiogenic than the bulk protolith. This may lead to melt extracted from a single source that evolves from mantle-like at the early stage to crustal-like after extensive melting. Mixing of magmas from different batches may mimic that of crustal- and mantle-derived magmas in terms of Hf isotopes. However, when the initial Zr content is close to or below 50 ppm, or zircon is absent in the protolith, such variation is limited and may not be recorded.

It has to be pointed out that this model considers only the two extreme conditions. If diffusive exchange of Hf during melting is negligible for most phases in the source, a full knowledge of the melting reactions and dissolution rate of each phase at the source is required to accurately reproduce the Hf isotopic evolution path. For example, garnet, if present, is an important reservoir of radiogenic ^{176}Hf, and the break-down of garnet during high-temperature dehydration melting (Wolf and Wyllie, 1994) may result in a sudden release of radiogenic ^{176}Hf into the melt.

5.6. "Zircon effect" in crustal anatexis: issues and implications

Zirconium is abundant in continental crust with the average concentrations ranging from 68 ppm in the lower crust to 193 ppm in the upper crust (Rudnick and Gao, 2003). This means that the zircon effect, as a result of slow disequilibrium melting of zircon, may be common during crustal melting. This may give rise to two issues. First, that the Hf isotope composition recorded in zircons that crystallize in a frequently recharged magma chamber may be highly variable. Second, that the Hf isotope compositions in the early melts may be highly radiogenic due to the retention of ^{177}Hf by zircon. The average Hf isotope composition recorded in granitic zircons may significantly deviate from that of the source.

These issues may substantially complicate the application of Hf isotopes when studying crustal magmatism, and make Hf isotopes a less reliable tracer especially when the source has a high Zr concentration or the melting is fast. This may shed light on the understanding of Hf isotopes in zircons from different types of granitic rocks due to the source diversity and thus large variation in Zr concentration at the source. Further work is needed to give a detailed comparison of zircon Hf isotope heterogeneity in different rock types. For the two samples (09JL-6-1 and 09JL-11-1) from the Jiuling Pluton, their different Hf isotopic heterogeneity may result from the varying melting conditions at the source e.g., melting degree, melting rate, etc. Therefore, Hf isotopic heterogeneity recorded by zircons in granitic rocks does not necessarily indicate multi-sourced magma mixing e.g., crust–mantle interaction at the magma source or magma chamber. A full understanding of the geological context plus careful field and petrographic study may help to distinguish between single-sourced disequilibrium melting and multi-sourced magma mixing. Our work suggests that isotopic heterogeneity observed in granitic rocks may be explained by disequilibrium melting as an alternative to multi-sourced magma mixing, especially when there is lack of clear field evidence of mixing.

The zircon effect may lead to Nd–Hf isotopic decoupling during the long-term crustal evolution which includes partial melting and high-grade metamorphism in the deep crust, and chemical weathering at the surface (Patchett et al., 1984; Zheng et al., 2008; Carpentier et al., 2009). Understanding disequilibria in crustal melting would allow further insights into the granitic magmatism, radiogenic isotope system evolution and crustal differentiation processes.

6. Conclusions

1) The five granitic samples analyzed in this work showed large variation in zircon $\varepsilon_{Hf}(t)$ (> 5 epsilon units), rough zircon Th/U–T correlation and no Lu/Hf–T correlation. The zircon $\varepsilon_{Hf}(t)$ values do not correlate with the Th/U ratios and is independent of T in zircons with reverse thermal zonation ($T_{rim} > T_{core}$). These observations suggest that these zircons likely grew in open systems.
2) Our modeling suggests that zircons may survive during crustal melting if the source has a relatively high Zr concentration (>100 ppm) or the melting is rapid ($> 10^{-4}$ yr^{-1}). Residual zircons may retain a significant amount of ^{177}Hf at the source.
3) Hf isotopic heterogeneity recorded in magmatic zircons of granitic rocks may not necessarily indicate magma mixing of multiple sources. The "zircon effect" during crustal anatexis results from disequilibrium melting of zircon at the source, and will lead to the production of isotopically distinct batches of melts that do not represent the bulk isotope composition of source.
4) The "zircon effect" may have commonly occurred during crustal anatexis given the generally high Zr concentration in crust. This may give rise to the decoupling between Hf and

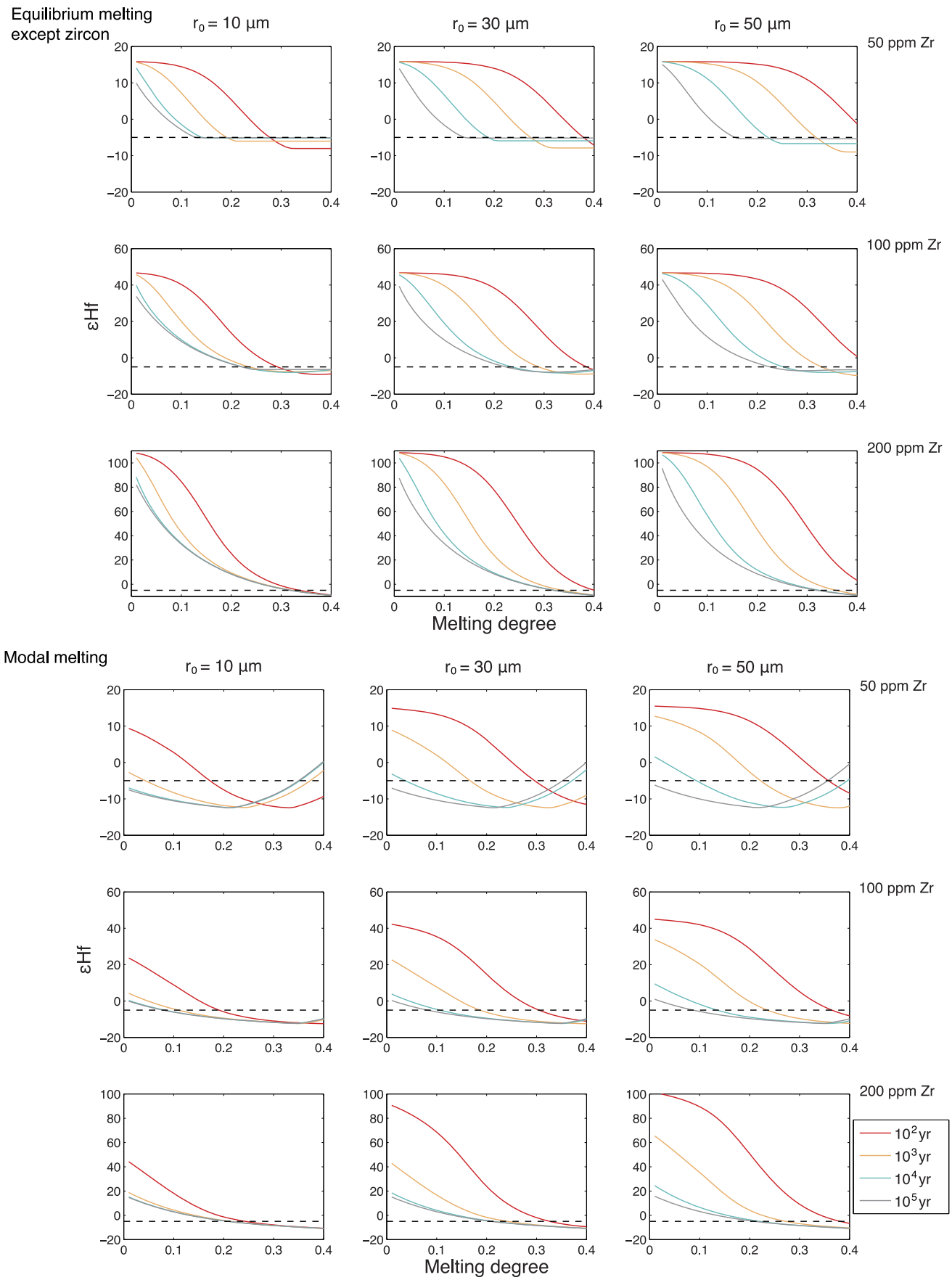

Fig. 7. Evolution of Hf isotopic composition in the extracted melt. Note the scale of ε_{Hf}-axis. The dashed lines indicate the ε_{Hf} value of the source prior to melting. The modal melting generally produces less variation because this melting model essentially assumes an effective bulk distribution coefficient of 1 for non-zircon Hf. In this extreme case, the radiogenic Hf (non-zircon Hf) is far less efficiently released from the source.

other radiogenic isotopic systems. In the context of crustal evolution, these findings may challenge the reliability of this tracer in at least some cases.

Acknowledgements

This work was financially supported by a 973 project of China (2012CB416701), the National Natural Science Foundation of China (Grant Nos. 41222016, 41072144), and New Century Excellent Talents in University (NCET-13-0281). We appreciate the thoughtful and constructive comments from the editor (T.M. Harrison), Prof. Calvin Miller, and two anonymous reviewers, who improved the paper greatly. We thank B. Wu for Laser U–Pb analyses, H.J. Gong for CL imaging and Prof. J.S. Qiu and Dr. Z. Li for providing samples from Zhejiang Province. This manuscript benefitted from discussions with Profs. Cin-Ty Lee, R.L. Rudnick, and R.J. Walker.

Appendix A. Supplementary material

Supplementary material related to this article can be found online at http://dx.doi.org/10.1016/j.epsl.2013.12.036.

References

Anczkiewicz, R., Szczepanski, J., Mazur, S., Storey, C., Crowley, Q., Villa, I.M., Thirlwall, M., Jeffries, T.E., 2007. Lu–Hf geochronology and trace element distribution in garnet: implications for uplift and exhumation of ultra-high pressure granulites in the Sudetes, SW Poland. Lithos 95, 363–380.

Ayres, M., Harris, N., 1997. REE fractionation and Nd-isotope disequilibrium during crustal anatexis: constraints from Himalayan leucogranites. Chem. Geol. 139, 249–269.

Bea, F., 1996. Residence of REE, Y, Th and U in granites and crustal protoliths: implications for the chemistry of crustal melts. J. Petrol. 37, 521–552.

Belousova, E.A., Griffin, W.L., O'Reilly, S.Y., 2006. Zircon crystal morphology, trace-element signatures and Hf-isotope composition as a tool for petrogenetic modeling: examples from eastern Australian granitoids. J. Petrol. 47, 329–353.

Blichert-Toft, J., Albarede, F., 1997. The Lu–Hf geochemistry of chondrites and the evolution of the mantle–crust system. Earth Planet. Sci. Lett. 148, 243–258.

Blundy, J.D., Wood, B.J., 1994. Prediction of crystal–melt coefficients from elastic moduli. Nature 372, 452–454.

Boehnke, P., Watson, E.B., Trail, D., Harrison, T.M., Schmitt, A.K., 2013. Zircon saturation re-revisited. Chem. Geol. 351, 324–334.

Carpentier, M., Chauvel, C., Maury, R., Mattielli, N., 2009. The "zircon effect" as recorded by the chemical and Hf isotopic compositions of the Lesser Antilles forearc sediments. Earth Planet. Sci. Lett. 287, 86–99.

Chen, B., Tian, W., Jahn, B.M., Chen, Z.C., 2008. Zircon SHRIMP U–Pb ages and in-situ Hf isotopic analysis for the Mesozoic intrusions in South Taihang, North China craton: evidence for hybridization between mantle-derived magmas and crustal components. Lithos 102, 118–137.

Chen, J.-Y., Yang, J.-H., Zhang, J.-H., Sun, J.-F., Wilde, S.A., 2013. Petrogenesis of the Cretaceous Zhangzhou batholith in southeastern China: zircon U–Pb age and Sr–Nd–Hf–O isotopic evidence. Lithos 162–163, 140–156.

Cherniak, D.J., Hanchar, J.M., Watson, E.B., 1997. Diffusion of tetravalent cations in zircon. Contrib. Mineral. Petrol. 127, 383–390.

Choi, S.H., Mukasa, S.B., 2012. Lu–Hf and Sm–Nd isotope systematics of Korean spinel peridotites: a case for metasomatically induced Nd–Hf decoupling. Lithos 154, 263–276.

Claiborne, L.L., Miller, C.F., Walker, B.A., Wooden, J.L., Mazdab, F.K., Bea, F., 2006. Tracking magmatic processes through Zr/Hf ratios in rocks and Hf and Ti zoning in zircons: an example from the Spirit Mountain batholith, Nevada. Mineral. Mag. 705, 517–543.

Claiborne, L.L., Miller, C.F., Flanagan, D.M., Clynne, M.A., Wooden, J.L., 2010a. Zircon reveals protracted magma storage and recycling beneath Mount St. Helens. Geology 38, 1011–1014.

Claiborne, L.L., Miller, C.F., Wooden, J.L., 2010b. Trace element composition of igneous zircon: a thermal and compositional record of the accumulation and evolution of a large silicic batholith, Spirit Mountain, Nevada. Contrib. Mineral. Petrol. 160, 511–531.

Davies, G.R., Tommasini, S., 2000. Isotopic disequilibrium during rapid crustal anatexis: implications for petrogenetic studies of magmatic processes. Chem. Geol. 162, 169–191.

Farina, F., Stevens, G., 2011. Source controlled $^{87}Sr/^{86}Sr$ isotope variability in granitic magmas: the inevitable consequence of mineral-scale isotopic disequilibrium in the protolith. Lithos 122, 189–200.

Flowerdew, M.J., Millar, I.L., Vaughan, A.P.M., Horstwood, M.S.A., Fanning, C.M., 2006. The source of granitic gneisses and migmatites in the Antarctic Peninsula: a combined U–Pb SHRIMP and laser ablation Hf isotope study of complex zircons. Contrib. Mineral. Petrol. 151, 751–768.

Fu, B., Page, F.Z., Cavosie, A.J., Fournelle, J., Kita, N.T., Lackey, J.S., Wilde, S.A., Valley, J.W., 2008. Ti-in-zircon thermometry: applications and limitations. Contrib. Mineral. Petrol. 156, 197–215.

Griffin, W.L., Wang, X., Jackson, S.E., Pearson, N.J., O'Reilly, S.Y., Xu, X.-S., Zhou, X.-M., 2002. Zircon chemistry and magma mixing, SE. China: in-situ analysis of Hf isotopes, Tonglu and Pingtan igneous complexes. Lithos 61, 237–269.

Hammouda, T., Pichavant, M., Chaussidon, M., 1994. Mechanisms of isotopic equilibrium during partial melting: An experimental test of the behavior of Sr. Mineral. Mag. 58, 368–369.

Hanyu, T., Tatsumi, Y., Nakai, S., Chang, Q., Miyazaki, T., Sato, K., Tani, K., Shibata, T., Yoshida, T., 2006. Contribution of slab melting and slab dehydration to magmatism in the NE Japan arc for the last 25 Myr: constraints from geochemistry. Geochem. Geophys. Geosyst. 7, Q08002. http://dx.doi.org/10.1029/2005GC001220.

Harrison, T.M., Watson, E.B., Aikman, A.B., 2007. Temperature spectra of zircon crystallization in plutonic rocks. Geology 35, 635–638.

Hayden, L.A., Watson, E.B., 2007. Rutile saturation in hydrous siliceous melts and its bearing on Ti-thermometry of quartz and zircon. Earth Planet. Sci. Lett. 258, 561–568.

Hoffmann, J.E., Münker, C., Polat, A., Rosing, M.T., Schulz, T., 2011. The origin of decoupled Hf–Nd isotope compositions in Eoarchean rocks from southern West Greenland. Geochim. Cosmochim. Acta 75, 6610–6628.

Hogan, J.P., Sinha, A.K., 1991. The effect of accessory minerals on the redistribution of lead isotopes during crustal anatexis: a model. Geochim. Cosmochim. Acta 55, 335–348.

Hoskin, P.W.O., Schaltegger, U., 2003. The composition of zircon and igneous and metamorphic petrogenesis. Rev. Mineral. Geochem. 53, 27–62.

Ickert, R.B., Williams, I.S., Wyborn, D., 2010. Ti in zircon from the Boggy Plain zoned pluton: implications for zircon petrology and Hadean tectonics. Contrib. Mineral. Petrol. 162, 447–461.

Jagoutz, O., Müntener, O., Ulmer, P., Pettke, T., Burg, J.P., Dawood, H., Hussain, S., 2007. Petrology and mineral chemistry of lower crustal intrusions: the Chilas Complex, Kohistan (NW Pakistan). J. Petrol. 48, 1895–1953.

Jochum, K.P., Weis, U., Stoll, B., Kuzmin, D., Yang, Q.-C., Raczek, I., Jacob, D.E., Stracke, A., Birbaum, K., Frick, D.A., Günther, D., Enzweiler, J., 2011. Determination of reference values for NIST SRM 610–617 glasses following ISO guidelines. Geostand. Newsl. http://dx.doi.org/10.1111/j.1751-908X.2011.00120.x.

Kemp, A.I.S., Hawkesworth, C.J., Foster, G.L., Paterson, B.A., Woodhead, J.D., Hergt, J.M., Gray, C.M., Whitehouse, M.J., 2007. Magmatic and crustal differentiation History of granitic rocks from Hf–O isotopes in zircon. Science 315, 980–983.

Kinny, P.D., Mass, R., 2003. Lu–Hf and Sm–Nd isotope systems in zircon. Rev. Mineral. Geochem. 53, 327–341.

Knesel, K.M., Davidson, J.P., 1996. Isotopic disequilibrium during melting of granite and implications for crustal contamination of magmas. Geology 24, 243–246.

Li, X.-H., Li, Z.-X., Ge, W.-C., Zhou, H.-W., Li, W.-X., Liu, Y., Wingate, M.T.D., 2003. Neoproterozoic granitoids in South China: crustal melting above a mantle plume at ca. 825 Ma? Precambrian Res. 122, 45–83.

Li, Z., Qiu, J.-S., Jiang, S.-Y., Xu, X.-S., Hu, J., 2009. Petrogenesis of the Jinshan granitic composite pluton in Fujian Province: constraints from elemental and isotopic geochemistry. Acta Geol. Sinica 83, 515–527 (in Chinese with English abstract).

Li, Z., Qiu, J.-S., Zhou, J.-C., 2010. Geochronology, geochemistry, and Nd–Hf isotopes of early Palaeozoic–early Mesozoic I-type granites from the Hufang composite pluton, Fujian, South China: crust–mantle interactions and tectonic implications. Int. Geol. Rev. 54, 15–32.

Miller, C.F., McDowell, S.M., Mapes, R.W., 2003. Hot and cold granites? Implications of zircon saturation temperatures and preservation of inheritance. Geology 31, 529–532.

Nebel, O., Jacobsen, Y.N., Mezger, K., Berndt, J., 2007. Initial Hf isotope compositions in magmatic zircon from early Proterozoic rocks from the Gawler Craton, Australia: a test for zircon model ages. Chem. Geol. 241, 23–37.

Nutman, A.P., 2006. Comment on "Zircon thermometer reveals minimum melting conditions on earliest Earth". Science 311, 779.

Patchett, P.J., White, W.M., Feldmann, H., Kienlinczuk, S., Hofmann, A.W., 1984. Hafnium/rare earth element fractionation in the sedimentary system and crustal recycling into the Earth's mantle. Earth Planet. Sci. Lett. 1984, 365–378.

Petford, N., Cruden, A.R., McCaffrey, J.W., Vigneresse, J.-L., 2000. Granite magma formation, transportation and emplacement in the Earth's crust. Nature 408, 669–673.

Qi, C.S., Deng, X.G., Li, W.X., Li, X.H., Yang, Y.H., Xie, L.W., 2007. Origin of the Darongshan–Shiwandashan S-type granitoid belt from southeastern Guangxi: geochemical and Sr–Nd–Hf isotopic constraints. Acta Petrol. Sinica 23, 403–412 (in Chinese with English abstract).

Qiu, J.-S., Li, Z., Liu, L., Zhao, J.-L., 2012. Petrogenesis of the Zhangpu composite granite pluton in Fujian Province: constraints from zircon U–Pb ages, elemental geochemistry and Nd–Hf isotopes. Acta Geol. Sinica 86, 561–576 (in Chinese with English abstract).

Roux, V.L., Bodinier, J.L., Alard, O., O'Reilly, S.Y., Griffin, W.L., 2009. Isotopic decoupling during porous melt flow: a case-study in the Lherz peridotite. Earth Planet. Sci. Lett. 279, 76–85.

Rubatto, D., Hermann, J., 2007. Experimental zircon/melt and zircon/garnet trace element partitioning and implications for the geochronology of crustal rocks. Chem. Geol. 241, 38–61.

Rudnick, R.L., Gao, S., 2003. Composition of the continental crust. In: Holland, H.D., Turekian, K.K. (Eds.), Treatise on Geochemistry, vol. 3, pp. 1–64.

Sawyer, E.W., 1994. Melt segregation in the continental crust. Geology 22 (11), 1019–1022.

Scherer, E., Munker, C., Mezger, K., 2001. Calibration of the lutetium–hafnium clock. Science 293, 683–687.

Shaw, S.E., Flood, R.H., 2009. Zircon Hf isotopic evidence for mixing of crustal and silicic mantle-derived magmas in a zoned granite pluton, eastern Australia. J. Petrol. 50, 147–168.

Shu, X.-J., Wang, X.-L., Sun, T., Dai, M.N., 2011. Zircon trace elements, U–Pb ages and Hf isotopes for the Mesozoic granites from the western Nanling Range, South China: implication for petrogenesis and W–Sn mineralization. Lithos 127, 468–482.

Shu, X.-J., Wang, X.-L., Sun, T., Chen, W.-F., Shen, W.-Z., 2013. Crustal formation in the Nanling Range, South China Block: Hf isotope evidence of zircons from Phanerozoic granitoids. J. Asian Earth Sci. 74, 210–224.

Sun, J.-F., Yang, J.-H., Wu, F.-Y., Li, X.-H., Yang, Y.-H., Xie, L.-W., Wilde, S.A., 2010. Magma mixing controlling the origin of the Early Cretaceous Fangshan granitic pluton, North China Craton: in situ U–Pb age and Sr-, Nd-, Hf- and O-isotope evidence. Gondwana Res. 120, 421–438.

Tappe, S., Pearson, D.G., Nowell, G., Nielsen, T., Milstead, P., Muehlenbachs, K., 2011. A fresh isotopic look at Greenland kimberlites: cratonic mantle lithosphere imprint on deep source signal. Earth Planet. Sci. Lett. 305, 235–248.

Tommasini, S., Davies, G.R., 1997. Isotopic disequilibrium during anatexis: a case study of contact melting, Sierra Nevada, California. Earth Planet. Sci. Lett. 148, 273–285.

Tuttle, O.F., Bowen, N.L., 1958. Origin of Granite in the Light of Experimental Studies in the System $NaAlSi_3O_8$–$KAlSi_3O_8$–SiO_2–H_2O. Mem. Geol. Soc. Amer., vol. 74.

Vervoort, J., Patchett, P., Söderlund, U., Baker, M., 2004. Isotopic composition of Yb and the determination of Lu concentrations and Lu/Hf ratios by isotope dilution using MC-ICPMS. Geostand. Geoanal. Res. 5, 1525–2027.

Wang, X.-L., Zhou, J.-C., Qiu, J.-S., Zhang, W.-L., Liu, X.-M., Zhang, G.-L., 2006. LA–ICP–MS U–Pb zircon geochronology of the Neoproterozoic igneous rocks from Northern Guangxi, South China: implications for tectonic evolution. Precambrian Res. 145, 111–130.

Wang, X.-L., Shu, X.-J., Xu, X.-S., Tang, M., Gaschnig, R., 2012. Petrogenesis of the Early Cretaceous adakite-like porphyries and associated basaltic andesites in the Jiangnan orogen, southern China. J. Asian Earth Sci. 61, 243–256.

Wang, X.-L., Zhou, J.-C., Wan, Y.-S., Kitajima, K., Wang, D., Qiu, J.-S., Sun, T., 2013. Magmatic evolution and Crustal recycling for Neoproterozoic strongly peraluminous granitoids from southern China: Hf and O isotopes in zircon. Earth Planet. Sci. Lett. 366, 71–82.

Watson, E.B., 1996. Dissolution, growth and survival of zircons during crustal fusion: kinetic principals, geological models and implications for isotopic inheritance. Trans. R. Soc. Edinb. Earth Sci. 87, 43–56.

Watson, E.B., Harrison, T.M., 1983. Zircon saturation revisited: temperature and composition effects in a variety of crustal magma types. Earth Planet. Sci. Lett. 64, 295–304.

Watson, E.B., Harrison, T.M., 2005. Zircon thermometer reveals minimum melting conditions on earliest Earth. Science 308, 841–844.

Wolf, M.B., Wyllie, P., 1994. Dehydration-melting of amphibolite at 10 kbar: the effects of temperature and time. Contrib. Mineral. Petrol. 115, 369–383.

Woodhead, J., Hergt, J., 2005. A preliminary appraisal of seven natural zircon reference materials for in situ Hf isotope determination. Geostand. Geoanal. Res. 29, 183–195.

Wu, R.-X., Zheng, Y.-F., Wu, Y.-B., Zhao, Z.-F., Zhang, S.B., Liu, X.-M., Wu, F.-Y., 2006. Reworking of juvenile crust: element and isotope evidence from Neoproterozoic granodiorite in South China. Precambrian Res. 146, 179–212.

Ye, M.-F., Li, X.-H., Li, W.-X., Liu, Y., Li, Z.-X., 2007. SHRIMP zircon U–Pb geochronological and whole-rock geochemical evidence for an early Neoproterozoic Sibaoan magmatic arc along the southeastern margin of the Yangtze Block. Gondwana Res. 12, 144–156.

Yu, C.-T., Zhang, F.-R., Huang, X.-S., 2006. Study on invasion mechanism of Jiuling Neoproterozoic granite. J. East China Inst. Tech. Suppl., 143–148.

Yu, S.-Y., Xu, Y.-G., Huang, X.-L., Ma, J.-L., Ge, W.-C., Zhang, H.-H., Qin, X.-F., 2009. Hf–Nd isotopic decoupling in continental mantle lithosphere beneath Northeast China: effects of pervasive mantle metasomatism. J. Asian Earth Sci. 35, 554–570.

Zeng, L.-S., Asimow, P.D., Saleeby, J.B., 2005a. Coupling of anatectic reactions and dissolution of accessory phases and the Sr and Nd isotope systematics of anatectic melts from a metasedimentory source. Geochim. Cosmochim. Acta 69, 3671–3682.

Zeng, L.-S., Saleeby, J.B., Asimow, P., 2005b. Nd isotopic disequilibrium during crustal anatexis: a record from the Goat Ranch migmatite complex, southern Sierra Nevada batholith, California. Geology 33, 53–56.

Zhang, S.-B., Zheng, Y.-F., Zhao, Z.-F., 2010. Temperature effect over garnet effect on uptake of trace elements in zircon of TTG-like rocks. Chem. Geol. 274, 108–125.

Zhao, L., Guo, F., Fan, W.-M., Li, C.-W., Qin, X.-F., Li, H.-X., 2010. Crustal evolution of the Shiwandashan area in South China: zircon U–Pb–Hf isotopic records from granulite enclaves in Indo-Sinian granites. Chin. Sci. Bull. 55. http://dx.doi.org/10.1007/s11434-010-3225-1.

Zheng, Y.F., Wu, R.X., Wu, Y.B., Zhang, S.B., Yuan, H.L., Wu, F.Y., 2008. Rift melting of juvenile arc-derived crust: geochemical evidence from Neoproterozoic volcanic and granitic rocks in the Jiangnan Orogen, South China. Precambrian Res. 163, 351–383.

Zhou, X.-M., Sun, T., Shen, W.-Z., Shu, L.-S., Niu, Y.-L., 2006. Petrogenesis of Mesozoic granitoids and volcanic rocks in South China: a response to tectonic evolution. Episodes 29, 26–33.

Zhu, K.-Y., Li, Z.-X., Xu, X.-S., Wilde, S.A., 2013. Late Triassic melting of a thickened crust in southeastern China: evidence for flat-slab subduction of the Paleo-Pacific plate. J. Asian Earth Sci. http://dx.doi.org/10.1016/j.jseaes.2013.01.010.